Physics

Physics Research Publications

Purdue University *Year* 2009

Doubly resonant Raman electron paramagnetic transitions of Cr3+ in ruby (Al2O3:Cr3+)

X. Lu S. Venugopalan H. J. Kim

M. Grimsditch S. Rodriguez A. K. Ramdas

Doubly resonant Raman electron paramagnetic transitions of Cr^{3+} in ruby ($Al_2O_3:Cr^{3+}$)

X. Lu,[1,*] S. Venugopalan,[2] Hyunjung Kim,[3] M. Grimsditch,[4] S. Rodriguez,[1] and A. K. Ramdas[1]
[1]*Department of Physics, Purdue University, West Lafayette, Indiana 47907, USA*
[2]*Department of Physics, SUNY-Binghamton, New York 13902, USA*
[3]*Department of Physics, Sogang University, Seoul 121-742, Korea*
[4]*Argonne National Laboratory, Argonne, Illinois 60439, USA*
(Received 12 March 2009; published 5 June 2009)

We report the Raman electron paramagnetic resonance (EPR) of Cr^{3+} in ruby ($Al_2O_3:Cr^{3+}$) in the $^4A_2$ (ground) and $\bar{E}$ (excited) states of its well-known R_1 emission line. Using tunable dye laser excitation within the range of the Zeeman components of R_1, we observe highly selective doubly resonant enhancements of the Raman EPR lines. The double resonances confirm the assignments of the Raman EPR lines, and they underscore the simultaneous occurrence of both "in resonance" and "out resonance" as visualized in the Kramers-Heisenberg quantum-mechanical picture of inelastic light scattering. The g factors of the $^4A_2$ and $\bar{E}$ states are consistent with the observed magnetic field dependence of the Raman EPR shifts. Through the interplay of Raman effect and the sharp Zeeman components of R_1, the results provide clear insights into the underlying microscopic mechanism of these resonant Raman EPR spectra of ruby.

DOI: 10.1103/PhysRevB.79.235204 PACS number(s): 78.20.Ls, 76.30.Fc, 78.40.Ha

I. INTRODUCTION

The incorporation of 3*d* transition-metal ions (TMIs) as substitutional impurities in host crystals, such as oxides (e.g., Al_2O_3, MgO) and II-VI semiconductors, leads to novel optical, semiconducting, magnetic, and magneto-optic properties.[1–3] These originate in the incomplete 3*d* electronic shell of TMI which gives rise to unique electronic levels, localized magnetic moments, and their possible exchange interactions with the band states of the host. The resulting fascinating physical phenomena in semiconductors are well exemplified in the class of materials known as diluted magnetic semiconductors (DMSs),[4,5] in which TMI randomly replace the group II cations in the lattice, causing tunable band gaps, large electronic g factors resulting in giant exciton spin splitting and Faraday rotation, as well as magnetic phase diagrams containing spin glass and antiferromagnetic phases, depending on the concentration of the TMI. Among the oxides, the Cr^{3+}-doped Al_2O_3, the well-known gemstone ruby, is a prime example of new physical properties originating from substitutional TMI impurity, replacing Al in this instance. Both the noteworthy red color of ruby, and its two sharp atomic-emission-like lines, known as R_1 and R_2, originate from the unique electronic structure[6–9] of the Cr^{3+} ion in ruby. The studies on the R_1 emission line of ruby have been central in several significant scientific advances, including the invention of the first laser[10] by Maiman in 1960. In all these cases, the nature of the electronic configurations of the TMI (i.e., $[Ar]3d^n4s^2$), their site symmetries in the host, spin-orbit interaction, and in some cases, the Jahn-Teller perturbations to which they are subjected when incorporated in the host have stimulated extensive basic and applied research.

In the present paper, we report the electronic Raman spectrum of ruby in which the electron paramagnetic resonance (EPR) within the Zeeman multiplet of the ground state of the R_1 line occurs as Stokes and anti-Stokes Raman shifts. We demonstrate doubly resonant effects in the Raman EPR spectra by tuning the incident photon energies across the spectral range in which the sharp Zeeman components of R_1 occur. These double resonances arise from the *simultaneous* occurrence of both "in resonance" and "out resonance" for Raman EPR lines of ruby, which follow naturally from the Kramers-Heisenberg[11] picture of Raman scattering. In such instances, the energies of both the incident photon ($\hbar\omega_L$) and the scattered photon ($\hbar\omega_S$) coincide with two different allowed electronic transitions of the medium, causing a pronounced enhancement of the intensities of the Raman lines, thanks to the resonance caused by both the denominator terms of the scattering cross section. Such double resonances were observed in DMS by Gubarev *et al.*[12] and in a molecular beam epitaxy (MBE)-grown bulk GaAs by Jayaraman *et al.*,[13] by tuning not only the exciting photon energy but also another experimental parameter (e.g., magnetic field, uniaxial or hydrostatic stress, temperature). However, the double-resonance effects reported here are entirely intrinsic to the electronic structure of Cr^{3+} in ruby, since they are realized *solely* by tuning the exciting radiation, without simultaneously tuning another experimental parameter to specific values. In other words, we demonstrate that whenever a Raman EPR line of ruby experiences an in resonance, inevitably it undergoes out resonance as well. This aspect also enables unambiguous assignments of the observed Raman EPR features of ruby and leads to clear insights into the mechanism of these resonant Raman EPR spectra.

II. EXPERIMENTAL

Raman and photoluminescence (PL) spectra were recorded using oriented single crystals of ruby placed in an optical cryostat incorporating a superconducting magnet. Spectra were obtained in the right-angle scattering geometry at a nominal sample temperature of 6 K. The low sample temperature allowed us to exploit the extremely small linewidth of R_1 and its Zeeman components near liquid-helium temperature, and thereby explore the resonance effects with

high sensitivity. PL spectra were excited using the 5145 Å line of an Ar^+ laser; below 1 T these spectra were recorded under high resolution ($\sim$0.01 cm^{-1}) of a piezoelectrically scanned, five-pass, Fabry-Perot interferometer. Above 1 T, both Raman and PL spectra were recorded with a double-grating spectrometer, with a resolution of $\sim$0.2 cm^{-1}. The chromium concentration of the samples is estimated to be $\sim 2.3\times 10^{19}$ cm^{-3}. The Raman spectra were excited with a dye laser with DCM dye as the lasing medium.[14] Optically pumped with the 5145 Å line of an Ar^+ laser, it provided an ideal continuously tunable source of monochromatic radiation in the range 6200–7400 Å, which includes the Zeeman components of R_1. All the spectra reported here were obtained with the magnetic field $\mathbf{B}\|\mathbf{c}$, the optic axis of ruby.

III. RESULTS AND DISCUSSION

We present and discuss our experimental results below in three parts. First, in part A, the PL spectra of R_1 and their magnetic field dependence are presented. These are relevant for the subsequent discussions on the Raman EPR spectra of ruby. Next, the Raman EPR spectra of the ground and excited states of R_1 are discussed, respectively, in parts B and C. In all three sections, the discussion is confined to the spectra obtained with $\mathbf{B}\|\mathbf{c}$. With $\mathbf{B}\perp\mathbf{c}$, level mixing effects arise in the ground-state Zeeman multiplet of R_1, and hence they are no longer pure spin states. For this reason, we will discuss our results for $\mathbf{B}\perp\mathbf{c}$ elsewhere in a future publication.

A. Photoluminescence spectra

Electronic levels of Cr^{3+} ions[6–9] occupying a trigonal site in Al_2O_3 and reflecting the effects of the trigonal distortion, crystal-field effects, and spin-orbit coupling give rise to strong absorption bands in the green (U band $\sim$18 000 cm^{-1}) and the blue (Y band $\sim$25 000 cm^{-1}) spectral ranges, thereby endowing ruby with its characteristic red color. Electrons optically excited into the broad U and the Y bands nonradiatively decay into the metastable $2\bar{A}$ and the $\bar{E}$ states. From $2\bar{A}$ and $\bar{E}$, electrons decay radiatively into the $^4A_2$ ground state, generating the sharp R_1 and R_2 lines, respectively, as shown in Fig. 1(a). The Zeeman splittings of $\bar{E}$ and $^4A_2$ for $\mathbf{B}\|\mathbf{c}$ produce the six photoluminescence transitions of R_1, i.e., (PL_2–PL_7), shown schematically in Fig. 1(b). These transitions appear strongly in the absorption spectrum of ruby as well. The R_1 and R_2 lines at zero field and their Zeeman components at 6 T with $\mathbf{B}\|\mathbf{c}$ are displayed in Fig. 2(a), while the magnetic field dependence of the six Zeeman components of R_1 ($PL_2,\ldots,PL_7$,) is shown in Fig. 2(b). The solid lines are calculated using the spin Hamiltonian[15] with $g_\parallel=1.984$ and $2D=-0.3824$ cm^{-1} for $^4A_2$ and $g_\parallel=2.45$ for the $\bar{E}$ excited state[16] based on microwave-EPR experiments. For convenience in further discussion, Table I lists the positions of the six Zeeman components of R_1 at $B=6$ T along with the initial and final states which give rise to each component.

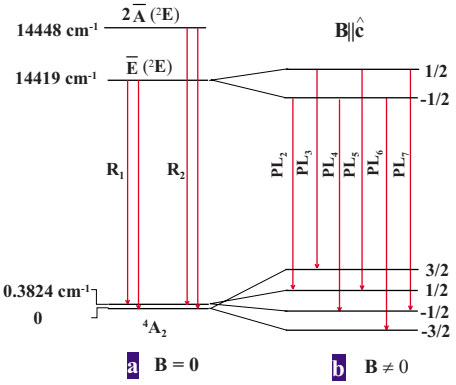

FIG. 1. (Color online) (a) The initial ($2\bar{A}$ and $\bar{E}$) and final states ($^4A_2$) of the R_1 and R_2 emission lines of Cr^{3+} in Al_2O_3:Cr^{3+} (ruby), respectively, shown schematically at zero magnetic field $\mathbf{B}$. (b) The Zeeman components of the R_1 emission line ($PL_2,\ldots,PL_7$,), shown schematically for $\mathbf{B}\|\mathbf{c}$.

B. Raman EPR of the $^4A_2$ (ground) state of R_1

Figure 3(a) shows the Raman EPR transitions within the $^4A_2$ Zeeman multiplet as Stokes and anti-Stokes shifts at 6 T with $\mathbf{B}\|\mathbf{c}$. The incident photon energy $\hbar\omega_L$ from the dye laser was 14397.5 cm^{-1} at 40 mW power. Note that although this $\hbar\omega_L$ lies below the lowest PL_n in Table I (i.e., PL_2), it is nonetheless close enough to the PL region. Indeed, with the same laser power, and $\hbar\omega_L$ lowered by only about 20 cm^{-1}, the intensities of the Raman lines decreased so drastically that they become almost unobservable. This indicates that the spectrum in Fig. 3(a) has already been considerably enhanced through near-resonant conditions. Positive and negative Raman shifts in the figure identify Stokes and anti-Stokes Raman lines, respectively. Each Stokes line has an anti-Stokes counterpart. The Raman *shifts* remain constant as $\hbar\omega_L$ is changed and are linear in B, as shown in Fig. 3(b).

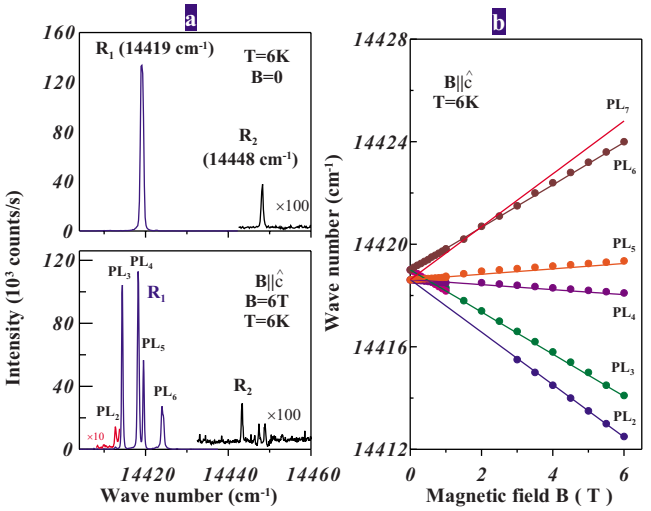

FIG. 2. (Color online) (a) The R_1 and R_2 emission lines of Cr^{3+} in ruby at zero magnetic field (upper part). The Zeeman components of the R_1 line ($PL_2,\ldots,PL_7$,) observed at 6 T with $\mathbf{B}\|\mathbf{c}$ (lower part). (b) Energies of the Zeeman components of the R_1 line as a function of $\mathbf{B}\|\mathbf{c}$.

TABLE I. Zeeman components of the R_1 line observed in the PL spectrum at $B=6$ T.

PL_n	Position (cm^{-1})	Assignment	
		$\bar{E}$	$^4A_2$
PL_2	14412.47	−1/2	1/2
PL_3	14414.07	1/2	3/2
PL_4	14418.03	−1/2	−1/2
PL_5	14419.25	1/2	1/2
PL_6	14423.97	−1/2	−3/2
PL_7	14424.81	1/2	−1/2

The straight lines are calculated from the spin Hamiltonian[15] with $g_{\|}=1.984$ and $2D=-0.3824$ cm^{-1}. It is evident that the observed Raman EPR shifts, denoted as full circles, are in excellent agreement with the calculated straight lines and clearly justify the assignments of the observed Raman lines. Thus, the new spectral features can be unambiguously ascribed to the $\Delta m=\pm 1$ and ± 2 Raman EPR transitions of Cr^{3+} within the $^4A_2$ multiplet. Raman lines $(-3/2\rightarrow -1/2)$ and $(-3/2\rightarrow 1/2)$ converge at $+2|D|$ for $B=0$, whereas those for $(-1/2\rightarrow 3/2)$ and $(1/2\rightarrow 3/2)$ do so at $-2|D|$ for $B=0$. We note that in Fig. 3(a) the expected $(-1/2\rightarrow 1/2)$ Stokes Raman transition and its corresponding anti-Stokes component have not been resolved from the nearby Raman lines; as will be seen below, they are observed distinctly only under the exact resonance conditions, and their magnetic field dependence falls on the line passing through the origin in Fig. 3(b).

Figure 4 shows the evolution of the Raman EPR spectrum as $\hbar\omega_L$ is tuned through the PL region, with the magnetic field being kept constant at 6 T. The occurrence of the pronounced resonance enhancement for each specific Raman

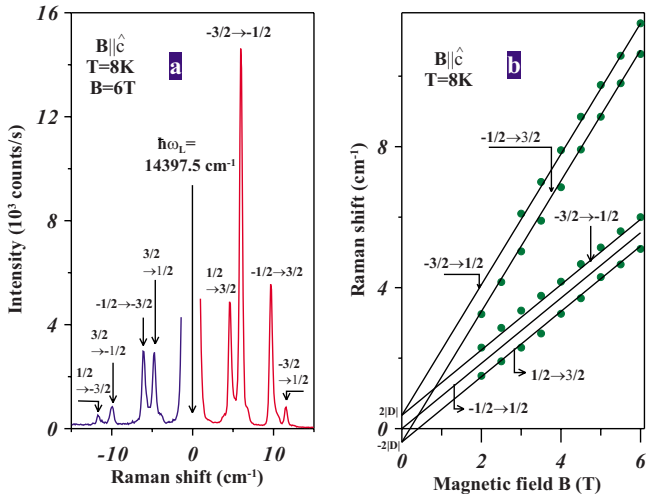

FIG. 3. (Color online) (a) Raman EPR of Cr^{3+} in ruby. The Stokes and the anti-Stokes Raman EPR shifts recorded with the incident photon energy $\hbar\omega_L$ at 14 397.5 cm^{-1}, $\mathbf{B}\|\mathbf{c}$, and $T=8$ K. (b) The Raman EPR transition energies as a function of $\mathbf{B}$. The straight lines are calculated results with the spin-Hamiltonian (Ref. 15) for $\mathbf{B}\|\mathbf{c}$.

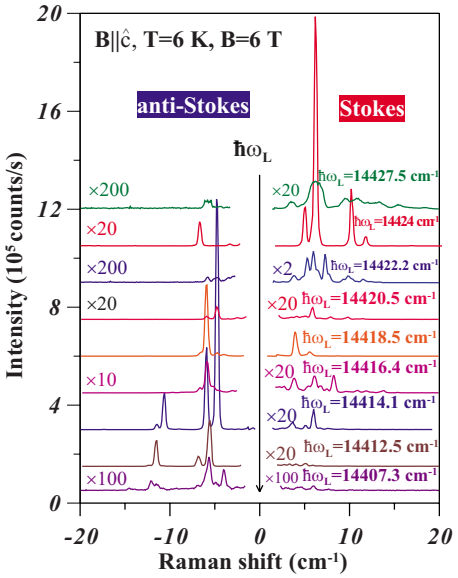

FIG. 4. (Color online) Raman EPR spectra of Cr^{3+} in ruby as a function of $\hbar\omega_L$ in the range of the Zeeman components of the R_1 line. $B=6$ T.

line as a function of $\hbar\omega_L$, in Stokes and/or anti-Stokes sides, is clearly evident in this figure. One can appreciate the sharpness of the resonance curve from the distinct intensity changes in a given Raman line, even for minute energy changes in $\hbar\omega_L$. When the incident radiation energy increases from low to high, spanning the energy range of the Zeeman components of R_1, the resonance enhancement occurs first for the anti-Stokes, then for the Stokes Raman EPR lines. For instance, with $\hbar\omega_L=PL_2$, the anti-Stokes Raman transitions $(1/2\rightarrow -1/2)$ corresponding to $\Delta m=-1$ and $(1/2\rightarrow -3/2)$ corresponding to $\Delta m=-2$ come into resonance, while the corresponding Stokes transitions are barely seen. Note also that when $\hbar\omega_L$ changes by just 2.3 cm^{-1}, from 14 414.1 to 14 416.4 cm^{-1}, the intensity of the anti-Stokes Raman transition $(3/2\rightarrow 1/2)$ decreases by 4 orders of magnitude. Eventually, with $\hbar\omega_L=PL_6$, the Stokes spectrum is stronger by 4 orders of magnitude compared to the anti-Stokes spectrum. It is clear that all these strong resonances are observed while $\hbar\omega_L$ is tuned over a narrow range of ~30 cm^{-1}, which overlaps the PL region. These experimental observations are considered below in further detail.

A Raman transition is visualized in the Kramers-Heisenberg theory[11,17] as a two-photon process: a virtual electric-dipole absorption involving the incident photon $\hbar\omega_L$ coupling the initial state $|g\rangle$ to an intermediate electronic state $|i\rangle$, and a virtual electric-dipole emission from coupling $|i\rangle$ to the final state $|f\rangle$ producing a scattered photon $\hbar\omega_S$. The net exchange of energy with the scattering system is thus (E_f-E_g), the Raman shift. From second-order perturbation theory, the scattering cross section for such a transition exhibits in resonance when $\hbar\omega_L=(E_i-E_g)$, whereas $\hbar\omega_S=(E_i-E_f)$ causes an out resonance; if both conditions are fulfilled simultaneously, a "double resonance" must occur, leading to the enormous intensity enhancement for the Raman transition involved. The possible intermediate states $|i\rangle$ in ruby may, in general, include the excited states of R_1, R_2, and the

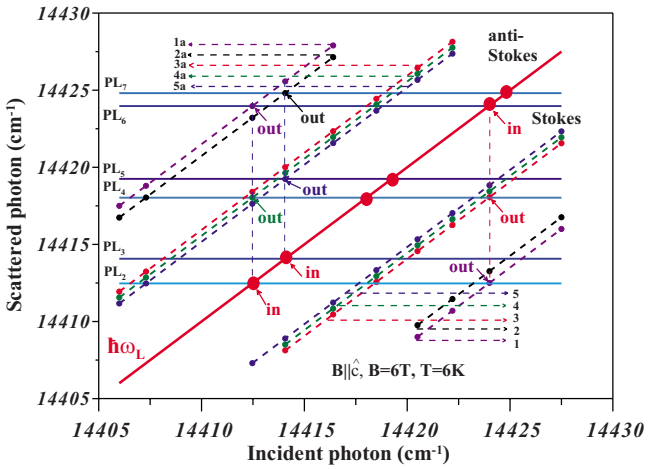

FIG. 5. (Color online) Scattered photon energies $\hbar\omega_S$ of Raman EPR lines as a function of the incident photon energy $\hbar\omega_L$. As a convenient reference line for the Stokes and the anti-Stokes Raman shifts, $\hbar\omega_L$ is also plotted along the diagonal of the figure, with all the $\hbar\omega_S$ lines, thus, being parallel to the diagonal $\hbar\omega_L$ line. The Raman transitions corresponding to each $\hbar\omega_S$ line (1a–5a and 1–5) are given in the text. Full circles on the $\hbar\omega_S$ lines denote the observed Raman shifts for $B=6$ T. The photoluminescence lines PL_2–PL_7, being independent of $\hbar\omega_L$, appear in the figure as horizontal lines parallel to the abscissa.

B levels as well as the U and Y bands.[7,8] However, the resonant effects are highly selective and lie within the range of the PL_2 to PL_7 (i.e., PL_n) features associated with R_1. Given the close proximity of the excited states of R_1 to the range of $\hbar\omega_L$ employed, one can justifiably identify the most relevant participating intermediate states for these Raman EPR spectra as the $\bar{E}(\pm\frac{1}{2})$ states.

Next, we pictorially illustrate how the double resonances arise. In Fig. 5, the ordinate corresponds to $\hbar\omega_S$ and the abscissa to $\hbar\omega_L$. Since the energies of the photoluminescence lines are independent of $\hbar\omega_L$ utilized in the Raman experiment, the positions of $PL_2,\ldots,PL_7$ appear in the figure as six horizontal lines parallel to the abscissa. Also, the diagonal line labeled as $\hbar\omega_L$ in this plot, corresponding to the incident photon energy, serves as a reference line for locating $\hbar\omega_S$, the Stokes $(1,\ldots,5)$ and the anti-Stokes shifts $(1a,\ldots,5a)$, for a given $\hbar\omega_L$; the $\hbar\omega_S$'s lie on lines parallel to $\hbar\omega_L$. The energies of the Raman lines with $\Delta m=\pm1$ and ±2 as a function of the tunable dye laser photon energy $(\hbar\omega_L)$ are also depicted on this plot. The labels (1a–5a and 1–5) of the Raman lines $(\hbar\omega_S)$ denote the following anti-Stokes Raman transitions within the $^4A_2$ Zeeman multiplet: $1a:(1/2\rightarrow-3/2)$; $2a:(3/2\rightarrow-1/2)$; $3a:(-1/2\rightarrow-3/2)$; $4a:(1/2\rightarrow-1/2)$; $5a:(3/2\rightarrow1/2)$; and their corresponding Stokes counterparts: $1:(-3/2\rightarrow1/2)$; $2:(-1/2\rightarrow3/2)$; $3:(-3/2\rightarrow-1/2)$; $4:(-1/2\rightarrow1/2)$; $5:(1/2\rightarrow3/2)$. As will be seen below, the above diagram allows one to discover unambiguously the $\hbar\omega_L$'s at which the resonant enhancements of the Raman EPR transitions occur.

The six intersections of the horizontal PL lines with the line labeled as $\hbar\omega_L$, denoted by full circles, thus identify the six incident photon energies for which the conditions for in resonance are fulfilled. Simultaneously, in each such case, there are only two Raman lines, both of which fulfill $\hbar\omega_S=E(PL_n)$, i.e., out resonance. These are two anti-Stokes lines, two Stokes lines, or one of each. These out resonances are signaled by the intersections of the $\hbar\omega_S$ lines with the PL lines (located at the vertical dashed lines passing through the corresponding full circle). Accordingly, we expect 12 occurrences of double resonance. The resulting selection rules at resonance, governing the $\Delta m=\pm1$ and ±2 Raman transitions, are listed in Table II for all the six possible cases of in resonance, for which $\hbar\omega_L=PL_n$. Each $\hbar\omega_L$ thus fulfills the condition for in resonance. Simultaneously, as Table II confirms, for each in resonance, there are only two allowed scattered photon transitions, whose energies naturally coincide with a PL_n and inevitably cause out resonances for two different Raman EPR lines. Thus a highly selective doubly resonant pair of Raman features is manifested. Although the Raman shifts and energies of PL_n are magnetic field dependent, it is clear from Table II that these double resonances

TABLE II. Selection rules for double resonance of Raman EPR lines.

$\hbar\omega_L$	$\hbar\omega_S$	Δm [Raman transition]
$^4A_2(1/2)\rightarrow\bar{E}(-1/2)=PL_2$	$\bar{E}(-1/2)\rightarrow{}^4A_2(-1/2)=PL_4$	$\Delta m=-1$ $[^4A_2(1/2)\rightarrow{}^4A_2(-1/2)]$
	$\bar{E}(-1/2)\rightarrow{}^4A_2(-3/2)=PL_6$	$\Delta m=-2$ $[^4A_2(1/2)\rightarrow{}^4A_2(-3/2)]$
$^4A_2(3/2)\rightarrow\bar{E}(1/2)=PL_3$	$\bar{E}(1/2)\rightarrow{}^4A_2(1/2)=PL_5$	$\Delta m=-1$ $[^4A_2(3/2)\rightarrow{}^4A_2(1/2)]$
	$\bar{E}(1/2)\rightarrow{}^4A_2(-1/2)=PL_7$	$\Delta m=-2$ $[^4A_2(3/2)\rightarrow{}^4A_2(-1/2)]$
$^4A_2(-1/2)\rightarrow\bar{E}(-1/2)=PL_4$	$\bar{E}(-1/2)\rightarrow{}^4A_2(-3/2)=PL_6$	$\Delta m=-1$ $[^4A_2(-1/2)\rightarrow{}^4A_2(-3/2)]$
	$\bar{E}(-1/2)\rightarrow{}^4A_2(1/2)=PL_2$	$\Delta m=+1$ $[^4A_2(-1/2)\rightarrow{}^4A_2(1/2)]$
$^4A_2(1/2)\rightarrow\bar{E}(1/2)=PL_5$	$\bar{E}(1/2)\rightarrow{}^4A_2(-1/2)=PL_7$	$\Delta m=-1$ $[^4A_2(1/2)\rightarrow{}^4A_2(-1/2)]$
	$\bar{E}(1/2)\rightarrow{}^4A_2(3/2)=PL_3$	$\Delta m=+1$ $[^4A_2(1/2)\rightarrow{}^4A_2(3/2)]$
$^4A_2(-3/2)\rightarrow\bar{E}(-1/2)=PL_6$	$\bar{E}(-1/2)\rightarrow{}^4A_2(-1/2)=PL_4$	$\Delta m=+1$ $[^4A_2(-3/2)\rightarrow{}^4A_2(-1/2)]$
	$\bar{E}(-1/2)\rightarrow{}^4A_2(1/2)=PL_2$	$\Delta m=+2$ $[^4A_2(-3/2)\rightarrow{}^4A_2(1/2)]$
$^4A_2(-1/2)\rightarrow\bar{E}(1/2)=PL_7$	$\bar{E}(1/2)\rightarrow{}^4A_2(1/2)=PL_5$	$\Delta m=+1$ $[^4A_2(-1/2)\rightarrow{}^4A_2(1/2)]$
	$\bar{E}(1/2)\rightarrow{}^4A_2(3/2)=PL_3$	$\Delta m=+2$ $[^4A_2(-1/2)\rightarrow{}^4A_2(3/2)]$

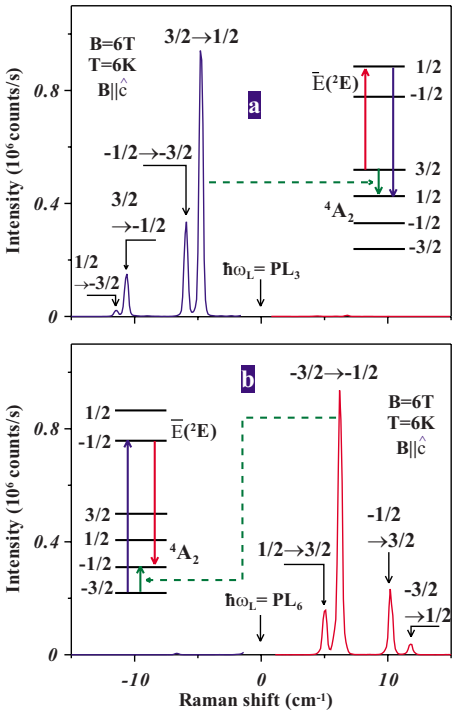

FIG. 6. (Color online) (a) The doubly resonant $^4A_2(3/2) \rightarrow {}^4A_2(1/2)$, $\Delta m=-1$ anti-Stokes Raman EPR line, and its two underlying electric-dipole-allowed transitions, which have transformed, under resonance, from "virtual" to "real" Kramers-Heisenberg transitions. (b) The doubly resonant $^4A_2(-3/2) \rightarrow {}^4A_2(-1/2)$, $\Delta m=+1$ Stokes Raman EPR line, and its two underlying Kramers-Heisenberg transitions.

will occur at *any* magnetic field. At any selected value of B, one merely has to tune $\hbar\omega_L$ so as to coincide with a specific PL_n; hence, no tuning of any other experimental parameter is involved. Figure 5 also shows that as $\hbar\omega_L$ is progressively increased, starting from below PL_2, selected anti-Stokes lines will first experience double resonance, followed by selected Stokes and anti-Stokes, and finally only selected Stokes lines. This is indeed consistent with the spectra shown in Fig. 4.

Next, we present experimental results which illustrate such double resonances for both anti-Stokes and Stokes Raman EPR transitions with reference to two specific cases listed in Table II, viz., $\hbar\omega_L=PL_3$ and $\hbar\omega_L=PL_6$. From Table II and Fig. 5, we note that when $\hbar\omega_L=PL_3={}^4A_2(3/2) \rightarrow \bar{E}(1/2)$, the resulting in resonance transforms the virtual electric-dipole absorption to a real transition; this is simultaneously accompanied by two real transitions in scattering $\bar{E}(1/2) \rightarrow {}^4A_2(1/2)$ and $\bar{E}(1/2) \rightarrow {}^4A_2(-1/2)$. Accordingly, the scattered photon energies coincide with PL_5 and PL_7, respectively, causing two out resonances. The corresponding anti-Stokes Raman EPR transitions within the $^4A_2$ Zeeman multiplet, which undergo double resonance, are the $\Delta m=-1:(3/2 \rightarrow 1/2)$ and the $\Delta m=-2:(3/2 \rightarrow -1/2)$ transitions. Indeed, in Fig. 6(a), the $(3/2 \rightarrow 1/2)$ and $(3/2 \rightarrow -1/2)$ anti-Stokes Raman lines have experienced such pronounced doubly resonant enhancements, while $(-1/2 \rightarrow -3/2)$ and $(1/2 \rightarrow -3/2)$ Raman features have also gained considerable intensity, being under near-resonant conditions; their intensities are nearly 2 orders of magnitude higher than those in Fig. 3(a). Note also that on the intensity scale of Fig. 6(a), the Stokes Raman spectrum is too feeble to be seen, unlike in Fig. 3(a). This is quite contrary to what one might expect from a normal thermal population factor; it is a manifestation of the huge double resonance experienced by these anti-Stokes features. Similarly, from Table II we note that the condition $\hbar\omega_L=PL_6$ will create an in resonance, which simultaneously causes out resonances corresponding to $\hbar\omega_S=\bar{E}(-1/2) \rightarrow {}^4A_2(-1/2)$ and $\bar{E}(-1/2) \rightarrow {}^4A_2(1/2)$; these scattered photon energies coincide, respectively, with PL_4 and PL_2, and correspond to the doubly resonant Stokes Raman EPR features with $\Delta m=+1$ and $+2$. This is confirmed in Fig. 6(b), where the $(-3/2 \rightarrow -1/2)$ and $(-3/2 \rightarrow 1/2)$ Stokes Raman lines have undergone doubly resonant enhancement, while their companion lines $(1/2 \rightarrow 3/2)$ and $(-1/2 \rightarrow 3/2)$ have also gained intensity through a near-resonant enhancement. Again, on the same intensity scale, the anti-Stokes Raman spectrum is invisible in Fig. 6(b). As indicated in Figs. 4 and 5, our experiments provide clear evidence of similar double resonances for other Raman EPR lines when $\hbar\omega_L$ is tuned through other PL_n.

It is worth noting that the in resonance and out resonance conditions may be separately satisfied in the range of the PL spectra as can be verified in Fig. 5 for *specific* Raman transitions. Furthermore, in Loudon's theory for Raman scattering by optical phonons in semiconductors,[18] the scattering process involves three steps in which the initial transition to the intermediate electronic level is separated from the final electronic transition by a matrix element involving electron-phonon interaction. A similar case of Raman EPR involving a TMI in the DMS occurs via a second step based on an exchange term.[19] As a result, the "in" and "out" resonances in such cases are not related energetically; however, the double resonances discussed here for ruby are clearly related energetically and occur without involving any intermediate step.

C. Raman EPR of the $\bar{E}$ (excited) state of R_1

It is possible to establish a steady-state electron population in the $\bar{E}$ (excited state) of R_1 when the sample is simultaneously illuminated with 2 mW of 5145 Å line of an Ar^+ laser. This causes the excitation of the U band and subsequent nonradiative decay from it to the $\bar{E}$ (excited state) of R_1. Figure 7 shows the Raman EPR spectrum obtained under these conditions with $\hbar\omega_L=14\ 395\ \text{cm}^{-1}$, $B=6$ T parallel to **c**, and $T=8$ K. A comparison of Figs. 3 and 7 shows that an additional Stokes as well as anti-Stokes Raman feature labeled as $\Delta\bar{E}(^2E)$ appears in Fig. 7. The inset of Fig. 7 shows the magnetic field dependence of this feature, which leads to a g factor of 2.43 ± 0.01, a value that is in excellent agreement with the known[16] $g_\parallel=2.445 \pm 0.001$ for the optically populated $\bar{E}$ (excited state) of R_1. Hence this new feature can be attributed to the Raman EPR of the $\bar{E}$ (excited state) of R_1. Furthermore, the measured angular dependence of the Raman shift of this feature, shown in Fig. 8, is in excellent

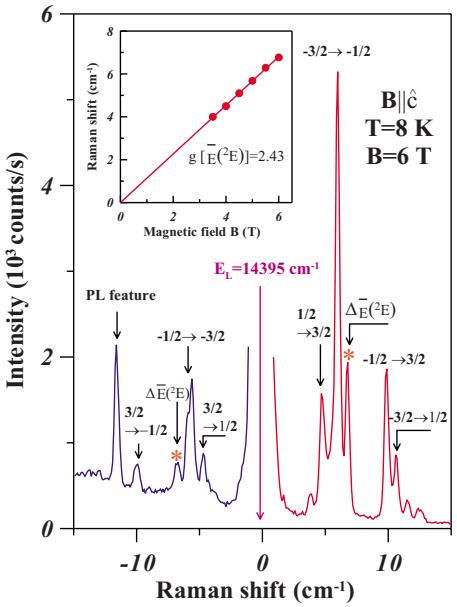

FIG. 7. (Color online) The Raman EPR transition between the Zeeman sublevels of the excited state $\bar{E}$ of R_1 is indicated by the asterisk and labeled as $\Delta\bar{E}(^2E)$. $\hbar\omega_L$=14 395 cm^{-1} with 40 mW power. The spectrum recorded at 6 T and 8 K with a simultaneous illumination of the sample by 5145 Å line of an Ar$^+$ laser. The inset shows the magnetic field dependence of the Raman feature $\Delta\bar{E}(^2E)$.

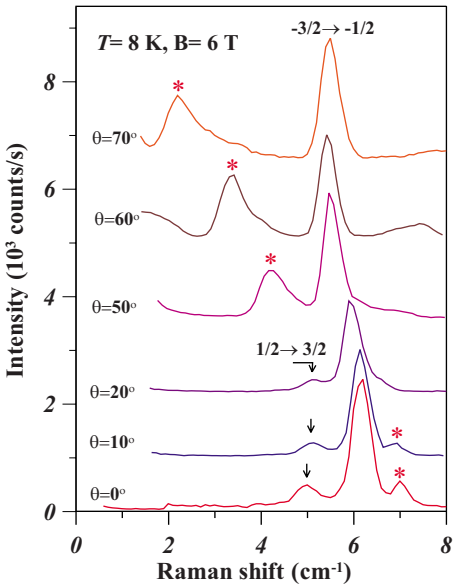

FIG. 8. (Color online) Raman spectra displaying the angular dependence of the $\Delta\bar{E}(^2E)$ Raman feature recorded at B=6 T and T=8 K; θ is the angle between **B** and **c**. The shifting position of the $\Delta\bar{E}(^2E)$ Raman feature with θ is indicated by the asterisks.

agreement with the expected angular dependence given by $g\mu_B B$, where $g=[(g_\parallel \cos\theta)^2+(g_\perp \sin\theta)^2]^{1/2}$, with $g_\parallel$=2.445, $g_\perp$=0.05, and θ= the angle between **B** and **c**.

IV. CONCLUDING REMARKS

In conclusion, we have successfully observed Raman EPR spectra associated with the ground-state $^4A_2$ Zeeman multiplet and $\bar{E}$ excited state of the R_1 line of ruby. The ground-state spectra show remarkably strong double resonances as the exciting radiation energy is swept through the region of the Zeeman components of R_1, as anticipated in the Kramers-Heisenberg picture of a Raman process. We also note that the conclusive assignments of features observed in Raman spectra are normally based on symmetry and accomplished through polarization measurements.[17] However, under resonant conditions, such selection rules are significantly violated,[20] and hence polarization measurements are not helpful in the assignment of the features. In this study, even without any polarization measurements, it has been possible to exploit the double resonances and unambiguously assign all the observed Raman EPR features to transitions which belong to specific initial, intermediate, and final states, thanks to the extremely selective role of the sharp Zeeman components of R_1.

ACKNOWLEDGMENTS

X.L., S.R., and A.K.R acknowledge support from the U.S. National Science Foundation (Grants No. DMR-0405082 and No. DMR-0705793), M.G. from the BES Material Sciences, U.S. Department of Energy (Grant No. W-31-109-ENG-38), and H.K. from Sogang University Special Research Grant (2008).

*Present address: Department of Physics, University of California, San Diego, La Jolla, CA 92093-0354.

[1] *Spectroscopy of Solid-State Laser-Type Materials*, edited by B. Di Bartolo (Plenum, New York, 1987).
[2] D. S. McClure, in *Solid State Physics*, edited by F. Seitz and D. Turnbull (Academic, New York, 1959), Vol. 9, p. 399.
[3] J. K. Furdyna, J. Appl. Phys. **53**, 7637 (1982); **64**, R29 (1988).
[4] *Diluted Magnetic Semiconductors*, edited by J. K. Furdyna and J. Kossut, Semiconductors and Semimetals Vol. 25 (Academic, San Diego, 1988), 276; T. Dietl, *Handbook of Semiconductors*, edited by S. Mahajan (Elsevier, Amsterdam, 1994), Vol. 3B, p. 1251.
[5] Eunsoon Oh, A. K. Ramdas, and J. K. Furdyna, J. Lumin. **52**, 183 (1992).
[6] K. H. Hellwege, *Einführung in die Festkörperphysik II*, (Springer-Verlag, Heidelberg, 1970). See in particular, Figs. 18.11 and 18.12 on pages 68 and 69, respectively.
[7] S. Sugano and Y. Tanabe, J. Phys. Soc. Jpn. **13**, 880 (1958); S. Sugano and I. Tsujikawa, *ibid.* **13**, 899 (1958).
[8] A. L. Schawlow, J. Appl. Phys. **33**, 395 (1962).

[9] F. Varsanyi, D. L. Wood, and A. L. Schawlow, Phys. Rev. Lett. **3**, 544 (1959).
[10] T. H. Maiman, Nature (London) **187**, 493 (1960).
[11] P. A. M. Dirac, *The Principles of Quantum Mechanics*, 4th ed. (Oxford University Press, Oxford, 1958), p.258.
[12] S. I. Gubarev, T. Ruf, and M. Cardona, Phys. Rev. B **43**, 1551 (1991).
[13] A. Jayaraman, G. A. Kouroulis, R. People, S. K. Sputz, and L. Pfeiffer, Pramana, J. Phys. **35**, 167 (1990).
[14] The ring dye laser, Model CR699, manufactured by Coherent Inc., 5100 Patrick Henry Dr., P.O. Box 54980, Santa Clara, CA 95054. DCM is the trade name for the organic dye [2-[2 [4-(dimenthylamino)phenyl]ethenyl 1]-6-methyl-4H-pyran-4-ylidene]-propanedintrile. This dye is sold, for example, by Exciton, Inc., P.O. Box 31126, Dayton, OH 45437-0126.
[15] A. A. Manenkov and A. M. Prokhorov, Sov. Phys. JETP **1**, 611 (1955), which gives the spin Hamiltonian, $\hat{H}=g_{\|}\mu_B B_z \hat{S}_z + g_{\perp}\mu_B(B_x\hat{S}_x+B_y\hat{S}_y)+D[\hat{S}_z^2-S(S+1)/3]$, $g_{\|}=1.984\pm0.0006$, $g_{\perp}=1.9867\pm0.0006$, μ_B=Bohr magneton, and $2D=-0.3824$ cm^{-1}.
[16] S. Geschwind, R. J. Collins, and A. L. Schawlow, Phys. Rev. Lett. **3**, 545 (1959).
[17] R. Loudon, *The Quantum Theory of Light*, 3rd ed. (Oxford University Press, Oxford, 2000), Chap. 8.
[18] R. Loudon, Proc. R. Soc. London, Ser. A **275**, 218 (1963).
[19] D. L. Peterson, D. U. Bartholomew, A. K. Ramdas, and S. Rodriguez, Phys. Rev. B **31**, 7932 (1985).
[20] W. Hayes and R. Loudon, *Scattering of Light by Crystals* (Dover, New York, 2004).